Electrical and photovoltaic properties of indium-tin-oxide/*p*-InSe/Au solar cells

J. Martínez-Pastor, A. Segura, and J. L. Valdés
Department de Fisica Aplicada, Facultad de Ciencias Fisicas, Burjasot, Valencia, Spain

A. Chevy
Laboratoire de Physique des Milieux très condensés, Tour 13, 4ème étage, 4 Place Jussieu, 75230 Paris Cedex 05, France

(Received 9 January 1987; accepted for publication 23 March 1987)

Conditions for efficiency improvement and optimization in indium-tin-oxide/*p*-indium-selenide solar cells are discussed in this paper. This aim is achieved by using low-resistivity *p*-indium-selenide and by incorporating a back-surface-field contact. This contact is insured by a *p*-indium selenide/gold barrier whose rectifying behavior is explained through the complex impurity structure of *p*-indium-selenide. Electrical and photovoltaic properties of the cells are also reported. The efficiency parameters under AM1 simulated conditions have been improved up to 32 mA/cm^2 for the short-circuit current density, 0.58 V for the open-circuit voltage, and 0.63 for the filling factor. As a result, solar efficiencies larger than 10% in annealed cells and 8% in unannealed ones have been attained. The limitations of these devices are discussed by investigating the dependence of electrical and efficiency parameters in function of photon flux and temperature.

I. INTRODUCTION

Among the layered semiconductors, indium-selenide (InSe) is the most suitable for photovoltaic conversion because of its energy gap (1.3 eV) and its optical and transport properties.[1,2] The largest solar collection for this semiconductor has been obtained in indium-tin-oxide (ITO)/*p*-InSe solar cells in which the short-circuit current can be as large as 25 mA/cm^2 (Ref. 2). The high resistivity of *p*-InSe[1,2] makes the filling factors lower than 0.4, and the compensated character of *p*-InSe limits the open-circuit voltage of 0.4 V. Therefore, the solar efficiency remains below 4%.[2,3]

The object of this work is to increase the efficiency of ITO/*p*-InSe solar cells by improving its electrical parameters. In order to achieve this aim, we have used samples from *p*-InSe ingots with lower resistivity, and we have incorporated a back-surface-field (BSF) contact to the cells. Part of the results have been briefly reported before.[4–6]

The electrical properties of *p*-InSe samples used are discussed in Sec. III. Section IV is devoted to the electrial properties of Au/*p*-InSe barriers. In Sec. V we report the $J(V)$ and $C(V)$ characteristics of ITO/*p*-InSe/Au devices, whose photovoltaic spectra are reported in Sec. VI. Solar efficiencies and limitations of the cells are studied in Sec. VII and VIII, respectively.

II. EXPERIMENT

p-InSe crystals were grown by the Bridgmann method from a polycrystalline melt of $In_{1.12}Se_{0.88}$ containing doping agents such as Zn, As, or Cd.[7] Table I (column 2) gives the percent of doping agent used in each growth.

ITO films were deposited by dc reactive sputtering in an air atmosphere (0.2 mm Hg) from a 95% indium–5% tin cathode. The substrate temperature was about 170 °C, and the target voltage was 1200 V. For these conditions the resistivity of the films is of the order of 10^{-3} Ω cm, and the electron concentration is about 10^{20} cm^{-3}. The thickness of the ITO layer was fixed at 65 nm for optimum antireflecting effect.

A number of cells were vacuum annealed at 150 °C for 4–5 h after depositing ITO, in order to improve the electrical characteristics of the film. The upper tin grid and the back gold contact were deposited by vacuum evaporation. Electrical characteristics $J(V)$ were measured with a curve tracer designed at the laboratory and a Tektronix 5023 digitizing oscilloscope. $C(V)$ characteristics were recorded at different frequencies by means of a system implemented at the laboratory consisting of a 3311A HP function generator, a 181 PAR current-sensitive preamplifier, a PAR 128A lock-in amplifier, and the Tektronix 5023 oscilloscope. Photovoltaic spectra were measured by using a Jobin Yvon H20 infrared (IR) monochromator. The source is a halogen burner with 3000-K radiation temperature. The beam is chopped at a frequency of 180 Hz by a PAR 125A modulator, and the photovoltage signal is amplified with a PAR 128A lock-in meter. All spectra in this report are at constant incident photon flux with the photovoltaic response corrected against the known absolute response of a Ge cell. Solar efficiency was measured under simulated AM1 flux and calibrated with a standard silicon cell.

III. ELECTRICAL PROPERTIES OF *p*-InSe

As-grown InSe is always *n*-type with an electron concentration of the order of 10^{15} cm^{-3}.[2,8] Then *p*-type InSe is a compensated semiconductor. Moreover, the high hole effective mass $m_h^* \approx 2m_0$ (Ref. 9) leads to low hole mobilities (about 25 cm^2/V s) and high acceptor-level ionization energies (about 250 meV).[10] Then a high acceptor concentration ($N_a \approx 5\times10^{16}$ cm^{-3}) is needed to get a room-temperature hole concentration of 10^{15} cm^{-3}. Recent transport measurements[11] have shown that the actual ionized impurity concen-

 0021-8979/87/161477-07$02.40

TABLE I. Transport properties of p-InSe ingots studied in this work.

	Ingot number	Doping agent	Impurity content concentration	$\rho_\perp$ (Ω cm)	$\rho_\parallel$ (Ω cm)	$\mu_\perp$ (cm^2/V s)	$\mu_\parallel$ (cm^2/V s)	p (cm^{-3})
Previous results		Zn		2×10^3	5×10^4	30	1.3	10^{14}
Present work	595/155	Zn	1000 ppm	150	2300	21	1.3	2×10^{15}
	498/73	Cd	0.93%	285	1300	22	5.0	10^{15}
	507/81	Cd	0.93%	140	1900	25	1.8	1.8×10^{15}
	524/94	As	1.3 ppm	150	1050	28	4.0	1.5×10^{15}

tration is, in fact, larger than 10^{17} cm^{-3} because there exists a self-compensating mechanism that creates deep donors located at about 0.6 eV above the valence band. A simple model for impurity structure in p-InSe is shown in Fig. 1.

This structure[5] seems to be the origin of the fact that this semiconductor makes good rectifying barriers with low work-function materials (like ITO), as well as with high work-function metals (like Pt or Au). In the first case the diode is a typical Schottky barrier with a depletion region (negative space charge). In the second case the barrier seems to be created by ionized deep donors, as we will discuss in Sec. IV.

In spite of these difficulties it was possible to obtain p-InSe with lower resistivity, as shown in Table I. These samples have resistivity along the layer, which has been reduced by a factor of 10 with respect to previously used ingots because of the increase of hole concentration. The resistivity across the layers is lowered by a factor of 50. The predominant scattering mechanism in this case is the scattering by potential barriers associated with planar defects parallel to the layers (stacking faults or impurity precipitates).[12] It seems that an increase in carrier densities leads to lower barrier height because of a screening effect, which would explain the fact that $\rho_\parallel$ decreases more than $\rho_\perp$.

IV. ELECTRICAL PROPERTIES OF Au/p-InSe BARRIERS

The inset of Fig. 3 shows the geometry of an Au/p-InSe/Sn device, where Sn acts as an ohmic contact.

This device exhibits a rectifying $J(V)$ characteristic (Fig. 2). The forward part is exponential with an ideality factor that ranges from 1.6 to 2.2 and typical saturation-current densities of the order of 10 μA/cm^2. The junction is forward biased when a positive voltage is applied to the Au contact. It means that p-InSe acts in this device as if it was n-type. This is, in principle, possible because the work function of Au is higher than the one of p-InSe. Nevertheless, the barrier so created (electrons would go from p-InSe to Au) should be a hole accumulation layer with an ohmic electrical characteristic. Thus the rectifying character of the Au/p-InSe junction cannot be explained if p-InSe contains only acceptor impurities.

Au/p-InSe barriers exhibit a $C(V)$ dependence typical of a Schottky barrier. Figure 3 shows the $C(V)$ characteristic corresponding to one of these devices made with Cd-doped p-InSe. It clearly appears that the $C(V)$ curve obeys the classical equation for abrupt barriers:

$$C^{-2}(V) = (V - V_{bi})/q\epsilon N_T, \tag{1}$$

where ϵ is the InSe low-frequency permittivity, V_{bi} is the built-in potential, and N_T is the impurity concentration of the deep level. The parameters of the barrier in this case are $V_{bi} \approx 0.3$ V, $N_T \approx 9\times10^{16}$ cm^{-3}, and $W \approx 0.06\,\mu$m.

As can be seen from these results, the ionized impurity concentration is two orders of magnitude higher than the hole concentration in the bulk material. The built-in potential makes the bulk material to be at an electrical potential of 0.3 V above the interface InSe/Au potential, which means that space charge must be positive in the depletion zone. Therefore, the ionized impurities should come from a deep donor level, and the barrier is formed because the electrons from this level are transferred to the gold, which incurves the bands so as to approach the Fermi level to the valence band.

The deep donor level predicted by Hall results is then confirmed by the electrical behavior of the Au/p-InSe barrier. This deep donor level appears in InSe independently of doping agent, and then the self-compensating mechanism seems to be an intrinsic response of this material when acceptor impurities are added.

V. ELECTRICAL PROPERTIES OF THE CELLS

According to the last discussion, the band scheme of ITO/p-InSe/Au solar cells would be the one shown in Fig. 4.

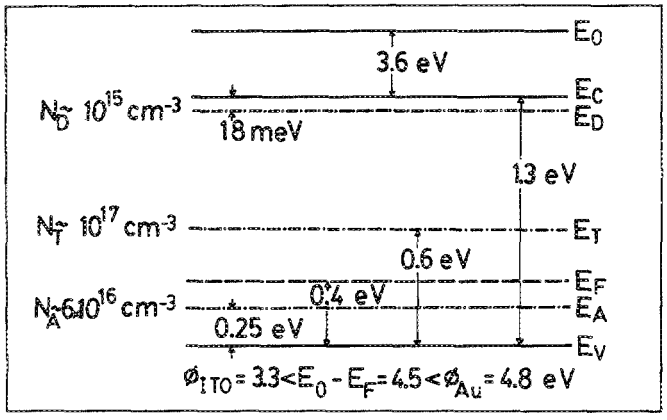

FIG. 1. Band structure model for p-InSe showing impurity levels; N_D and E_D: the concentration and energy of the shallow donor level; N_T and E_T: the concentration and energy of the deep donor level; N_A and E_A: the concentration and energy of the acceptor level; and E_0, E_c, E_F, and E_v: the energies of vacuum level, conduction band, Fermi level, and valence band, respectively.

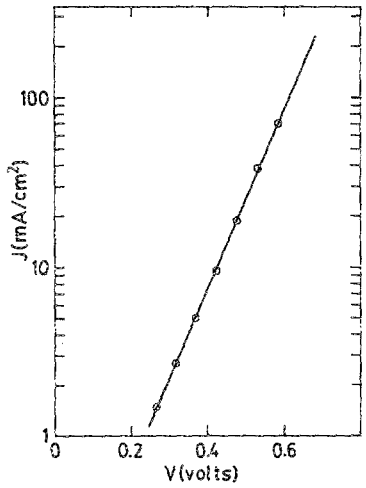

FIG. 2. Typical $J(V)$ characteristic of Au/p-InSe junction.

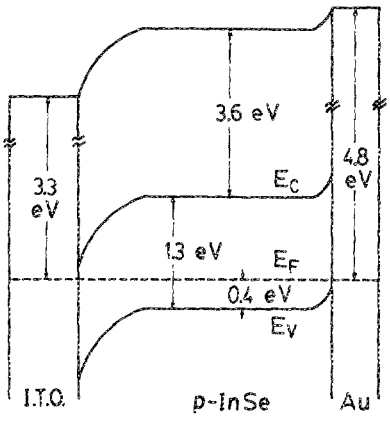

FIG. 4. Band scheme for ITO/p-InSe/Au devices.

The ITO/p-InSe contact is a typical Schottky barrier. If all impurity levels are occupied, then the donors are neutral, and the acceptors are negative, which results in a negative space charge. In the p-InSe/Au contact all impurity levels are empty; then the donors are positive and the acceptors are neutral, which results in a positive space charge. Therefore, this contact creates a back surface field.

Figure 5 shows the $J(V)$ characteristics in the dark of an old ITO/p-InSe:Zn/In cell (curve a) and two of the best ITO/p-InSe:As/Au cells (curves b and c). In Table II we have listed the electrical parameters A, J_s, and R_s for these cells and several others as computed from a fit to the equation

$$V = AkT/q \ln(J/J_s + 1) + JR_s. \quad (2)$$

The improvement in the electrical characteristics in the new cells with respect to the old ones is clear: (1) The saturation-current density of the ITO/p-InSe/Au cells has been decreased by nearly two orders of magnitude because of the back-surface-field contact. (2) The low resistivity of the p-InSe ingots used results in a reduction of series resistance R_s by more than 40 times. The poorest electrical characteristics correspond to cells prepared with Cd-doped material. On the other hand, annealing does not apparently improve the electrical parameters of the cells (curve b in Fig. 5).

An analysis of $J(V)$ characteristics in the dark with increasing temperature from 20 to 80 °C has been made in order to study the variation of saturation-current density J_s. The arrhenius plot of J_s versus the inverse temperature gives an activation energy of about 300 meV. This behavior indicates that the saturation current is controlled by a generation-recombination process due to deep levels in the depletion zone. A quantitative analysis is not possible without a more precise model of impurity levels in this material.

A typical $C^{-2}(V)$ plot, recorded at 100 Hz, of ITO/p-InSe:As/Au devices is shown in Fig. 6. It also obeys Eq. (1), where N_T must be substituted by N_a. The electrical parameters of the barrier are ionized-acceptor impurity concentration, $N_a \approx 2\times10^{15}\,\mathrm{cm}^{-3}$, built-in potential, $V_{bi} \approx 0.8$ V, and space-charge width, $W \approx 0.7\,\mu$m. As can be seen from these results, the ionized-acceptor impurity concentration is of the order of the hole concentration in thermal equilibrium in the bulk material. The ITO/p-InSe barrier is forward biased when a positive voltage is applied to the ITO contact, and therefore, the results are consistent with the impurity model proposed in Fig. 1 and band scheme in Fig. 4.

Figure 7 shows the capacitance at zero bias versus frequency for two ITO/p-InSe/Au cells. Its dependence with frequency reveals the presence of several deep levels, the transition frequencies between constant capacitance regions corresponding to the emission rates[15] of these levels. These curves confirm the complexity of impurity structure in p-

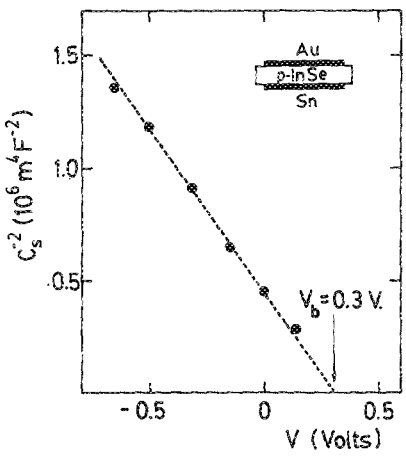

FIG. 3. $C^{-2}(V)$ plot corresponding to an Au/p-InSe barrier.

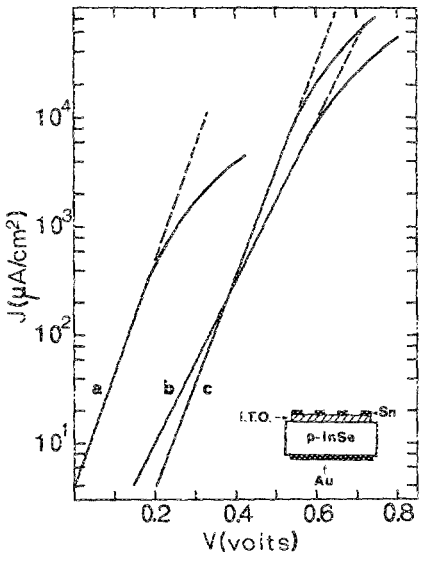

FIG. 5. $J(V)$ characteristics of several devices; curve a: ITO/p-InSe:Zn/Sn cell; curve b: annealed ITO/p-InSe:As/Au cell (10A-2); curve c: unannealed ITO/p-InSe:As/Au cell (6A-2).

TABLE II. Electrical parameters A, J_s, and R_s for several ITO/p-InSe solar cells.

Device	J_s (μA/cm^2)	A	R_s (Ω cm^2)
Previous results	4	1.6	60
5Z-5	0.14	2.05	2.1
PCd1-13	2.4	2.4	3.0
PCd2-1	3.8	2.88	2.9
6A-2	0.038	1.7	1.4
10A-2[a]	0.35	2.2	2.0

[a] Annealed at 150 °C.

InSe. The energies and cross section of deep levels have been measured by deep-level transient spectroscopy and will be reported elsewhere.[14]

$C(V)$ characteristics are frequency dependent. In a wide range of frequencies one observes an increase of the apparent built-in potential and the slope of the $C^{-2}(V)$ curve with increasing frequency, consistent with the fact that deeper levels cannot follow the higher frequencies.[13]

In a narrow range of frequencies where zero bias capacitance is constant, only the apparent built-in potential changes, as shown in Fig. 8 for a ITO/p-InSe:Cd/Au cell. This effect is due to series resistance, and the actual built-in potential is related to the apparent one through the equation[15]

$$V_{bi} = V_{bi}^{a} - q\epsilon N_i r^2 w^2. \tag{3}$$

V_{bi}^{a} and V_{bi} are the apparent and actual built-in potentials, respectively, N_i is the ionized impurity concentration, r is the series resistance in the bulk material, and w is the frequency.

In the inset of Fig. 9 the variation of the apparent built-in potential V_{bi}^{a} vs w^2 is shown, and we can see that the extrapolation of the resulting straight line gives the actual built-in potential $V_{bi} = 0.65$ V. If we add to V_{bi} the energy distance between the valence band and the Fermi level (about 300 meV), we can estimate a barrier height of the order of 0.95 eV for the ITO/p-InSe:Cd junction. The $C(V)$ characteristics also indicate that As-doped InSe gives higher

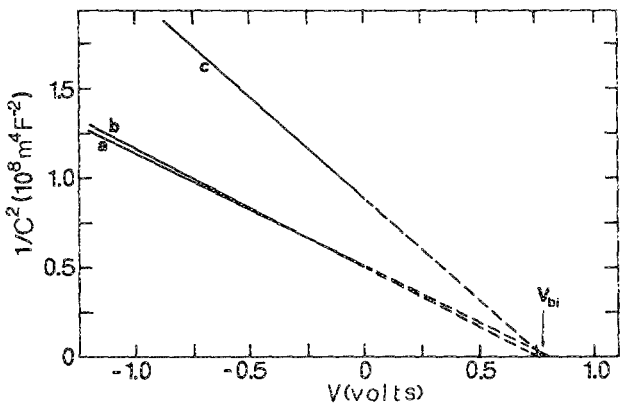

FIG. 6. $C^{-2}(V)$ plot for several ITO/p-InSe:As/Au devices at 100 Hz; curve a: 8A-6; curve b: 8A-2; and curve c: 8A-4.

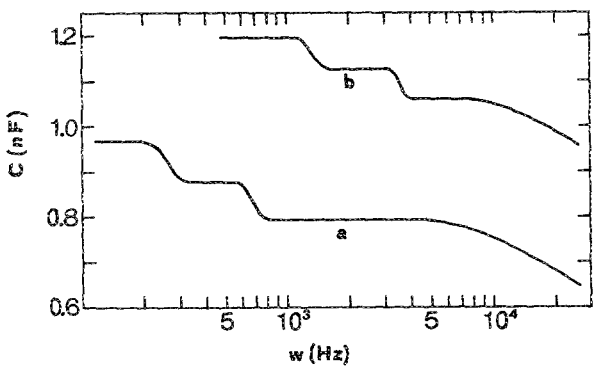

FIG. 7. Capacitance versus frequency at zero bias of two solar cells, (a) 8A-5 and (b) PCd2-1.

er built-in potentials with ITO ($V_{bi} \leqslant 0.8$ V) than Cd- or Zn-doped InSe ($V_{bi} \leqslant 0.65$ V).

As regards annealing, it does not seem to affect the barrier parameters of ITO/p-InSe:As junctions.

VI. PHOTOVOLTAIC PROPERTIES OF ITO/p-InSe/Au CELLS

A simple form to compute the external spectral response in our devices can be derived by integrating the number of photoexcited carriers that reach the junction.[16] The lower the recombination velocity at the back contact, the better this aproximation, which can be used in our case because of the presence of a BSF contact (zero recombination velocity).

In the calculation the contribution of light reflected from the back surface is taken into account by assuming the Au electrode to be totally reflecting. The ITO film is assumed to be transparent in the wavelength region between 1 and 3 eV. The surface effects have been accounted for by introducing a perturbed layer of thickness δ that does not contribute to the photocurrent. Then the external quantum efficiency of the devices is given by

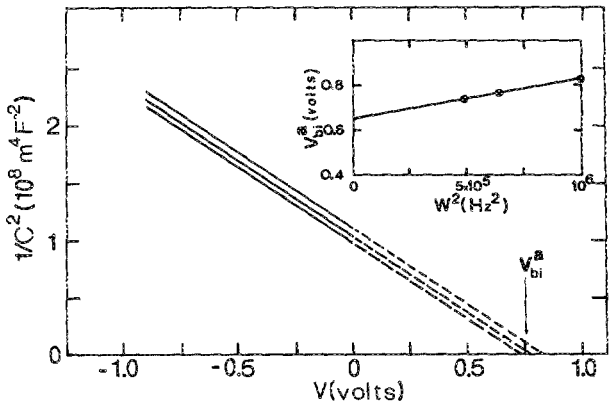

FIG. 8. $C^{-2}(V)$ curves of the PCd2-1 device for several frequencies: 700, 800, and 1000 Hz. The inset shows the apparent built-in potential vs square frequency.

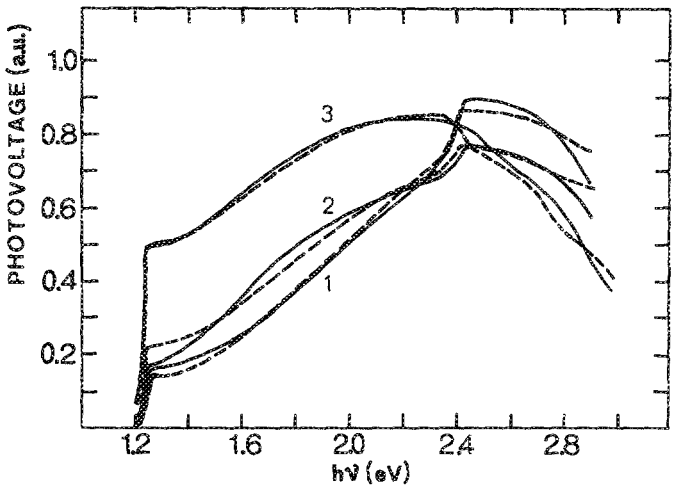

FIG. 9. Photovoltaic spectra for three devices; curve 1: 1Z-0; curve 2: PCd1-13 (507/81 ingot); and curve 3: PCd2-1 (498/73 ingot).

$$\eta(h\nu) = [1 - R(h\nu)]\{\exp(-\alpha\delta) - \exp(-\alpha W) + \exp(-2\alpha e)[\exp(\alpha W) - \exp(\alpha\delta)] + \alpha L/(\alpha L + 1)\{\exp(-\alpha W) - \exp[-\alpha e - (e - W)/L]\} + \alpha L/(\alpha L - 1)\exp(-\alpha e)\{\exp[(W - e)/L] - \exp(-\alpha e + \alpha W)\}\}, \quad (4)$$

where L is the minority-carrier difussion length, δ is the perturbed layer thickness, e is the cell thickness, W is the space-charge width, and α is the absorption coefficient:

$$R(h\nu) = \frac{R_1^2 + R_2^2 + 2R_1R_2\cos\theta}{1 + R_1^2R_2^2 + 2R_1R_2\cos\theta}, \quad (5)$$

where $R_1 = (n_1 - 1)/(n_1 + 1)$, $R_2 = (n_2 - n_1)/(n_2 + n_1)$, $\theta = 2n_1d_1\sigma$, n_1 is the refractive index of ITO, taken as 2,[17–20] n_2 is the refractive index of InSe from Ref. 21, and d_1 is the thickness of the ITO layer.

Figure 9 shows the photovoltaic spectra at constant photon flux of an ITO/p-InSe:Zn/Au cell (curve 1) and two ITO/p-InSe:Cd/Au cell (curves 2 and 3). Figure 10 shows the photovoltaic spectra of two ITO/p-InSe:As/Au cells (curve 1: unannealed cell, 10 μm thick; curve 2: annealed cell, 20 μm thick). In Table III we have listed the parameters that give the best least-squares fit to Eq. (4). Dotted lines in both Figs. 9 and 10 are the calculated spectra with these parameters. From Fig. 9 and Table III it appears that minority-carrier diffusion lengths are very low in Zn- and Cd-(507/81) doped ingots. It can be seen from Fig. 10 that the annealed cell (curve 1) exhibits a clear improvement in the photovoltaic spectrum: It has a photoresponse about 10% higher in the gap region for curve 2. It is due to a larger diffusion length (14 μm in the annealed cell and 11.2 μm in the unannealed one). This effect may be attributed to the fact that thick samples are less damaged during the cleavage and has been observed in other InSe devices.[2]

TABLE III. Photovoltaic parameters of some ITO/p-InSe/Au devices, corresponding to the best fit to Eq. (4).

Device	L (μm)	δ (μm)	e (μm)	d_1 (μm)	W (μm)
1Z-0	2.0	0.015	10.3	0.065	0.5
PCd1-13	1.4	0.020	23.0	0.065	0.5
PCd2-1	10.0	0.060	15.8	0.070	0.5
6A-2	11.2	0.040	10.6	0.065	0.7
10A-2[a]	14.0	0.060	21.0	0.065	0.7

[a] Annealed at 150 °C.

VII. SOLAR EFFICIENCY

Figure 11 shows the $J(V)$ characteristics of six devices under simulated AM1 conditions, corresponding to an old ITO/p-InSe:Zn/In cell, in comparison to four ITO/p-InSe/Au cells, one from each ingot studied, and an annealed ITO/p-InSe:As/Au cell. Table IV gives the efficiency parameters. During the test, the devices were in thermal contact with a copper block, maintained at room temperature ($\approx$293 K).

We can see that an important improvement with respect

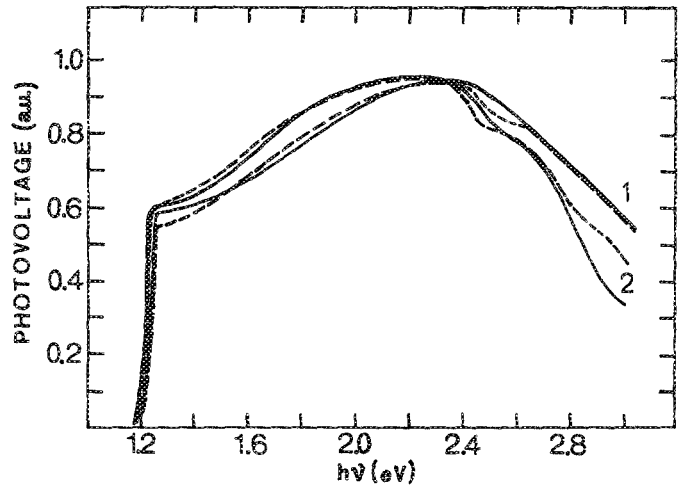

FIG. 10. Photovoltaic spectra for two ITO/p-InSe:As/Au devices; curve 1: unannealed cell (6A-2); curve 2: annealed cell (10A-2).

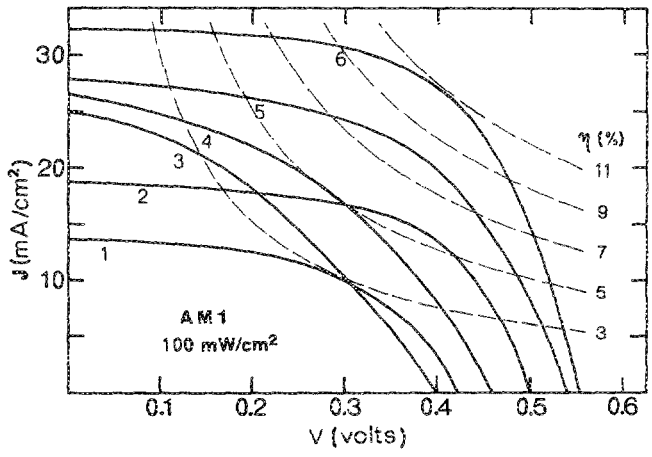

FIG. 11. $J(V)$ characteristics under simulated AM1 conditions at room temperature; curve 1: PCd1-13; curve 2: 5Z-5; curve 3: previous results; curve 4: PCd2-1; curve 5: 6A-2; and curve 6: 10A-2 (annealed cell).

TABLE IV. Efficiency parameters for several solar cells.

Device	e (μm)	S_a (mm^2)	J_{sc} (mA/cm^2)	V_{oc} (V)	FF	η (%)
Previous results	13.0	10.00	25.0	0.40	0.38	3.8
1Z-3	14.5	2.70	21.1	0.43	0.49	4.9
5Z-5	9.0	2.10	18.8	0.50	0.59	6.0
PCd1-13	23.0	1.12	13.7	0.42	0.53	3.0
PCd2-1	15.8	3.82	26.6	0.46	0.42	5.1
5A-6	14.5	2.43	27.6	0.54	0.45	7.2
6A-2	11.0	1.40	28.0	0.54	0.53	8.0
8A-3	13.0	1.66	24.4	0.58	0.46	6.5
9A-1	15.8	4.70	23.4	0.51	0.58	6.9
10A-2[a]	21.0	2.85	32.2	0.56	0.61	10.9
10A-3[a]	23.6	2.10	29.4	0.54	0.63	10.0

[a] Annealed at 150 °C.

to previous results is obtained in all cases, which is because of the lower resistivity of p-InSe and the BSF contact. The cells based on Zn- or Cd-doped InSe have lower V_{oc} and J_{sc} consistently with the measured lower barrier heights, lower minority-carrier diffusion lengths, and higher saturation-current density. The best results correspond to the As-doped material. Among the As-doped cells, the highest efficiencies are obtained with annealed thick cells ($d \approx 20$ μm). The higher J_{sc} is consistent with the larger diffusion length, but the better efficiency parameters cannot be related to the dark electrical parameters, which are of the same order as in the other As-doped cells.

VIII. LIMITATIONS OF THE ITO/p-InSe CELLS

In order to elucidate the origin of the limitations of these cells and to evaluate the possibilities of further improvements, we have studied the dependence of all the electrical and efficiency parameters on the photon flux. From $J(V)$ characteristics as a function of the photon flux, we have obtained the variation of the saturation-current density J_s, the series resistance R_s, and the ideality factor A as a function of the photon flux for the best ITO/p-InSe:As/Au device [Fig. 12(a)]. Figure 12(b) shows the variation of the open-circuit voltage V_{oc}, the filling factor FF, and the solar efficiency versus photon flux for the same cell. The short-circuit current density is strictly linear on the photon flux and has not been plotted.

From Fig. 12 we can clearly see the origin of the limitations of ITO/p-InSe cells. The saturation-current density increases with increasing photon flux up to a factor of 100 from its dark value in AM1 conditions. This causes V_{oc} not to increase logarithmically with photon flux, as it should, and also causes the filling factor to decrease. The reduction of the series resistance does not compensate this effect.

It must be pointed out that the increase of saturation-current density is the main factor contributing to the filling-factor decrease, the series resistance having little effect. This conclusion is also confirmed by the higher filling-factor values of the annealed ITO/p-InSe:As/Au cells, because their typical saturation-current density under illumination is about ten times lower than in unannealed ones.

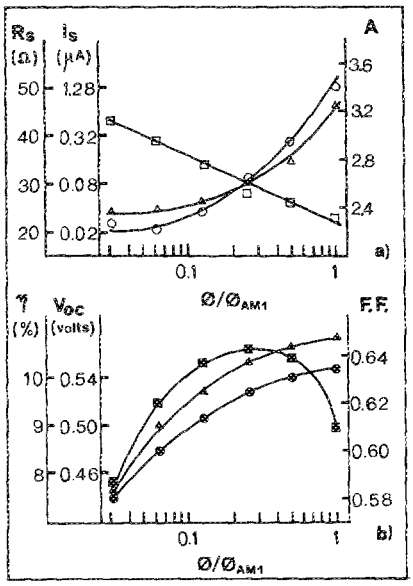

FIG. 12. (a) Electrical and (b) efficiency parameters of the 10A-2 cell: □: series resistance; △: saturation current; ○: ideality factor; ▩: filling factor; ▲: efficiency; and ●: open-circuit voltage.

Figure 13 shows the short-circuit current density J_{sc} as a function of the open-circuit voltage V_{oc} for four cells. As can be seen from curves 1 and 2 (corresponding to 9A-1 and 10A-2 cells, at room temperature), the open-circuit voltage would be about 150 mV higher if the electrical parameters did not change with respect to their dark value when the cell is illuminated. This reduction makes the solar efficiency decrease by about 25% from the ideal value. The origin of this behavior is due to the compensated character of p-InSe. In fact, this effect is stronger in p-InSe ingots with lower hole concentration, which is the case of As-doped InSe used in Bi/p-InSe devices,[2] where the hole concentration was of the order of 10^{13} cm^{-3}. Curve 4 in Fig. 13 corresponds to one of these devices. The open-circuit voltage saturates and even decreases at high values of photon flux.

The effect of illumination on saturation-current density has been studied as a function of temperature; $J(V)$ characteristics under AM1 conditions for a ITO/p-InSe:As/Au

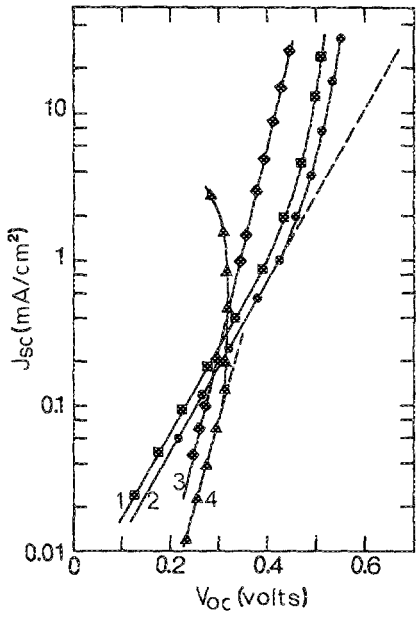

FIG. 13. Short-circuit current density vs open-circuit voltage for several devices; curve 1: 9A-1; curve 2: 10A-2; curve 3: 10A-3 (at 80 °C); and curve 4: Bi/p-InSe/Sn cell.

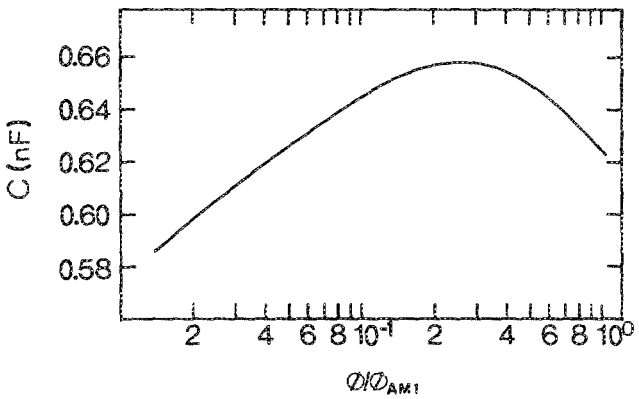

FIG. 14. Capacitance vs photon flux of an ITO/*p*-InSe:As/Au cell (10A-3).

cell (10A-3) at different temperatures (20–80 °C) have then been recorded and analyzed. The filling factor FF and short-circuit current density J_{sc} are nearly constant in all temperatures. The open-circuit voltage V_{oc} decreases with increasing temperature at a rate of about 1.83 mV/deg. The solar efficiency also decreases by 20% (at 80 °C) from its value at room temperature.

The saturation-current density under solar illumination turns out to be constant in the whole temperature range, leading to a constant filling factor. In fact, at 80 °C the saturation-current density does not change under illumination. Once more the effect of photon flux on the saturation current appears to be weaker when the hole concentration is higher (at 80 °C p can be as high as 5×10^{16} cm^{-3}). As a result, the $J_{sc}(V_{oc})$ dependence at 80 °C remains exponential in the whole photon flux range (curve 3 in Fig. 13).

These results can be explained through the impurity structure of *p*-InSe. The saturation of V_{oc} at high photon flux corresponds to a decrease of the ITO/*p*-InSe barrier height. The space charge being formed by negative ionized acceptors, this effect should be related to a decrease of negative-charge concentration because of the compensation of ionized acceptor by ionized deep donors. This effect can be observed through capacitance measurement under illumination. From Eq. (1) the capacitance of the cell under illumination should increase with increasing photon flux as

$$C\propto[N_i/(V_{bi}-V_{oc})]^{1/2}. \quad (6)$$

Figure 14 shows the capacitance of an ITO/*p*-InSe/Au cell in function of the photon flux. It clearly appears that the capacitance saturates and, after, decreases for the photon flux levels at which the open-circuit voltage also saturates. A complete explanation of this effect must include knowledge of the capture cross section of deep donors in InSe. According to our results, the concentration of ionized deep donors increases under illumination, which indicates that the capture cross section of these centers for electrons must be very low. In some way this overcompensated *p*-InSe becomes "*n*-type" under illumination, which lowers the built-in potential of the ITO/*p*-InSe junction and makes the saturation-current density increase.

IX. CONCLUSIONS

In this work we have shown that is is possible to improve and optimize the ITO/*p*-InSe structure and attain efficiencies higher than 10%. In spite of the poor electrical properties of *p*-InSe, short-circuit current densities, open-circuit voltages, and filling factors up to 32 mA/cm^2, 0.58 V, and 0.63, respectively, have been obtained. The main factors contributing to these results are (i) the lower resistivity of the material, (ii) the back-surface-field structure, (iii) the larger minority-carrier diffusion lengths in As-doped *p*-InSe, (iv) the optimization of substrate thickness, and (v) the thermal annealing of the devices.

The most important limitation of these devices is the increase of the saturation current under illumination, which makes the open-circuit voltage 25% lower than its ideal value. This limitation arises from the existence in *p*-InSe of a self-compensating mechanism that creates deep donors located below the middle of the band gap. Further studies on the nature and origin of these defects must be carried out in order to determine whether they appear as the results of an intrinsic property of the material or if they can be avoided by changing the growth conditions or the doping procedures.

ACKNOWLEDGMENTS

This work was supported through Spanish Government CAICYT under Grant No. 644/81.

[1] A. Segura, J. P. Guesdon, J. M. Besson, and A. Chevy, Rev. Phys. Appl. **14**, 253 (1979).
[2] A. Segura, J. P. Guesdon, J. M. Besson, and A. Chevy, J. Appl. Phys. **54**, 876 (1983).
[3] A. Segura, J. L. Valdés, F. Pomer, A. Cantarero, and A. Chevy, in *Proceedings of the 5th E.C. Photovoltaic Solar Energy Conference*, Kavouri, 1983 (Reidel, Dordrecht, 1984), p. 927.
[4] A. Segura, J. L. Valdés, A. Cantarero, F. Pomer, J. P. Martinez, B. Marí, and A. Chevy, in *Proceedings of the 6th European Communities Photovoltaic Solar Energy Conference*, Londres, 1985 (Reidel, Dordrecht, 1985), p. 774.
[5] A. Segura, J. L. Valdés, A. Cantarero, F. Pomer, J. P. Martinez, B. Marí, and A. Chevy, in *Proceedings of the MELECON*, Madrid, 1985. (Elsevier, New York 1985), p. 51.
[6] A. Segura, J. P. Martinez, J. L. Valdés, and A. Chevy, in *Proceedings of the 7th European Communities Photovoltaic Solar Energy Conference*, Sevilla 1986 (Reidel, Dordrecht, 1987), p. 475.
[7] A. Chevy, thèse d'etat, Université de Paris VI, 1981.
[8] A. Segura, K. Wünstel, and A. Chevy, Appl. Phys. A **31**, 139 (1983).
[9] A. Bourdon, A. Chevy, and J. M. Besson, in *Proceedings of the 14th International Conference on Physics of Semiconductors*, Edinburgh, 1978, Institute of Physics Conference Series No. 43, edited by B. L. H. Wilson (Institute of Physics, Bristol, 1979), p. 1371.
[10] S. Shigetomi, T. Ikari, Y. Koga, and S. Shigetomi, Jpn. J. Appl. Phys. **20**, L343 (1981).
[11] A. Segura (unpublished).
[12] R. C. Fivaz and Ph. E. Schmid, in *Optical and Electrical Properties* (Reidel, Dordrecht, 1976), p. 343.
[13] G. I. Roberts and C. R. Crowell, J. Appl. Phys. **41**, 1767 (1970).
[14] A. Segura (unpublished).
[15] A. M. Goodman, J. Appl. Phys. **34**, 329 (1963).
[16] S. M. Sze, *Physics of Semiconductor Devices* (Wiley, New York, 1969).
[17] D. B. Fraser and H. D. Cook, J. Electrochem. Soc. **119**, 1368 (1972).
[18] H. K. Mueller, Phys. Status Solidi **27**, 723 (1968).
[19] C. E. Wickersham and J. E. Greene, Phys. Status Solidi **47**, 329 (1978).
[20] J. C. Fan and F. J. Bachner, J. Electrochem. Soc. **122**, 1719 (1975).
[21] R. LeToullec, N. Piccioli, and J. C. Chervin, Phys. Rev. B **22**, 6162 (1980).